Current Density Induced in the Human Body due to Power Distributions Lines using the Boundary Element Method

Andrés Peratta, Cristina González, and Dragan Poljak

Abstract: **The paper presents the human exposure assessment to Extremely Low Frequency fields (ELF) by means of the three dimensional Boundary Element Method (BEM). The formulation is based on a rather realistic representation of the human body. The paper analizes the response of the density current due to variations on the detail of the conceptual model considered. Variations on the geometry model and the inclusion of organs have been considered. The results obtained with and without considering the rough representations of the internal organs were compared. This comparison allows to estimate their relevance in numerical modellings at ELF.**

I. INTRODUCTION

The increasing number of telecommunication and power systems makes the problem of exposure to the related electromagnetic (EM) fields more and more important. Either for protection from these fields, for optimisation purposes or for taking advantage of their possitive effects in treating or monitoring some particular diseases all the effects thermal and genetic have to be well established. In this area numerical modelling plays an important role, however major difficulties (as for example finding the correct physical properties of the different human tissues, or developing reliable numerical algorithms capable of yielding accurate and stable solutions for large number of degrees of freedom in order to represent as much as possible the real EM-thermal picture) need to be resolved and form part of many current research streams. Computational bioelectromagnetics can be classified into two groups of problems: low frequency in which electric and magnetic fields are decoupled, and high frequency in which energy absortion from electromagnetic radiation is dominant. For the human body the "high frequency problem" arises at frequencies around $10kHz$ due to the high values of permittivity of biological tissues. The first models which have been developed are 1D, treating the human geometry as ellipsoids or discs and with constant material properties. Although inaccurate and too simplified those models were used to define the safety standards and guidelines of the ICNIRP for the exposure levels of reference [1]. Two dimensional models gave more realistic results [2],[3]. However, 3D models remain necessary. Some of them have already been developed, see for example [4], [5], [6] and [7].

Boundary element methods (BEM) [8] have an attractive advantage for these large scale problems since they tend to avoid volume meshes and also their formulation is based on the fundamental solution of the leading operator for the governing equation, therefore being more accurate than standard Finite Element or Finite Difference methods. A similar approach has been successfully implemented for simpler geometries [9], and other BEM calculations have been implemented

in [10]. This paper deals with a realistic model of the human body on the Boundary Element analysis. The problem is formulated by the Laplace equation version of the continuity equation. Solving the corresponding Laplace equation for scalar potential via the BEM, the current density produced inside the body is obtained. Some illustrative computational results are presented in the paper.

This paper is organised in the following way: Section 2 outlines the mathematical background and the fundamentals of BEM. Section 3 shows the results for a 3D model representing the grounded human body underneath a power distribution line in terms of electric field and induced currents. Finally, the corresponding concluding remarks are elaborated in section 4.

II. METHODOLOGY

A. Electromagnetic Analysis

The physical model under study contemplates a grounded, isolated or semi-isolated human being and the air in its near environment such as the case shown in Figure 1. At low frequencies, the electric
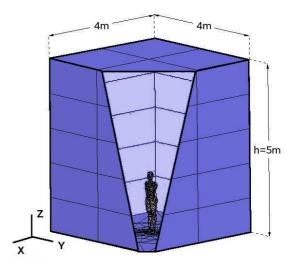

Fig. 1. Plan view of the integration domain in the near field. Distances are in meters

field **E** and magnetic field **H** are decoupled. When considering the human exposure to high voltage and low intensities systems, such as transmission lines, the most influential field is the electric one. So, directly from Maxwell's equations [11], under these assumptions, and considering that the conductivity σ, and the permittivity ϵ are constants within the considered region it is found that the electric scalar potential u obeys the following Laplace equation for the air

A. Peratta, C. González are both with Wessex Institute of Technology, Southampton, England, UK.

D. Poljak is with Department of Electronics - University of Split, Split, Croatia (e-mail: dragan.poljak@fesb.hr)

and the human body:

$$\nabla \cdot [(\sigma + i\omega\epsilon)\nabla u] = 0 \qquad (1)$$

where ω is the frequency of the incident field, and ϵ is the permittivity. At ELF frequencies biological tissues behave as good conductors with conductivity values of the order of $0.5 S/m$, and electric permittivity $10^{-10} F/m$, i.e. $\epsilon_r \sim 100$; and the air is a good dielectric. [12] ,[13], [14].

B. The boundary element solution of Laplace equation

This section provides a general overview of the BEM implemented for the solution of the ELF problem (Laplace equation)[15].

1) Integral Formulation: The numerical implementation of the BEM requires the discretisation of the domain boundary into elements, and this represents one of the most powerful advantages of the method, since there is no need to discretise in volume. The starting point of the BEM is the integral formulation of the governing differential equation. Consider the Laplace equation valid in Ω with an arbitrary source term

$$\nabla^2 u = 0 \qquad (2)$$

with the following conditions prescribed on $\Gamma = \Gamma_1 + \Gamma_2$ (the boundary of Ω) ,

$$u = \bar{u} \qquad \text{on} \quad \Gamma_1, \qquad (3)$$

$$\frac{\partial u}{\partial n} = \bar{q} \qquad \text{on} \quad \Gamma_2 \qquad (4)$$

where n is the normal to the boundary Γ. Then, weighting of (2) with function u^* becomes:

$$\int_\Omega (\nabla^2 u) u^* d\Omega = \int_{\Gamma_2} \left(\frac{\partial u}{\partial n} - \bar{q}\right) u^* d\Gamma - \int_{\Gamma_1} (u - \bar{u})\frac{\partial u^*}{\partial n} d\Gamma \qquad (5)$$

and integration by parts of the last expression yields

$$\int_\Omega u (\nabla^2 u^*) d\Omega = -\int_{\Gamma_2} \bar{q}u^* d\Gamma - \int_{\Gamma_1} \frac{\partial u}{\partial n} u^* d\Gamma$$
$$+ \int_{\Gamma_2} u\frac{\partial u^*}{\partial n} d\Gamma + \int_{\Gamma_1} \bar{u}\frac{\partial u^*}{\partial n} d\Gamma \qquad (6)$$

The weight function u^* is chosen to be the free space Green function of the Laplace operator, thus satisfying the following equation for a point source located at $\mathbf{x_i}$:

$$\nabla^2 u^* + \delta(\mathbf{x} - \mathbf{x}_i) = 0 \qquad (7)$$

Consequently, the former integral expression (6) can be written as:

$$c_i u_i + \int_\Gamma \frac{\partial u^*}{\partial n} u d\Gamma - \int_\Gamma u^* \frac{\partial u}{\partial n} d\Gamma \qquad (8)$$

where

$$c_i = \begin{cases} 1, & \text{if} \quad \mathbf{x_i} \in \Omega \\ 1/2, & \text{if} \quad \mathbf{x_i} \in \Gamma \quad \text{(smooth boundary)} \end{cases} \qquad (9)$$

Equation (8) represents the integral formulation of (2), and is the starting point of the BEM code that has been implemented.

2) Boundary discretisation: The first three terms in eq. (8) involve boundary-only integrals. The boundary Γ can be discretised into N_e boundary elements, so that

$$\Gamma = \sum_{j=1}^{N_e} \Gamma_j.$$

$$c_i u_i + \sum_{j=1}^{N_e} \int_{\Gamma_j} \frac{\partial u^*}{\partial n} u \, d\Gamma - \sum_{j=1}^{N_e} \int_{\Gamma_j} u^* \frac{\partial u}{\partial n} \, d\Gamma = 0 \qquad (10)$$

Each boundary element contains a number (N_{fn}) of collocation nodes, where the potential or normal fluxes are evaluated. In this way, the values of the potential or its normal derivative at any point defined by the local coordinates (ξ_1, ξ_2) on a given boundary element can be defined in terms of their values at the collocation nodes, and the N_{fn} interpolation functions ψ_k with $k = 1, N_{fn}$ in the following way:

$$u(\xi) = \sum_{k=1}^{N_{fn}} \psi_k(\xi) u_k, \qquad (11)$$

$$\frac{\partial u(\xi)}{\partial n} = \sum_{k=1}^{N_{fn}} \psi_k(\xi) \left.\frac{\partial u}{\partial n}\right|_k \qquad (12)$$

By discretising the boundary and applying the collocation technique, eq. (8) can be rewritten in the following way:

$$c_i u_i + \sum_{j=1}^{N_e} \sum_{k=1}^{N_{fn}} \left(\int_{\Gamma_j} \frac{\partial u^*}{\partial n_j} \psi_k d\Gamma_j\right) u_{kj} -$$
$$\sum_{j=1}^{N_e} \sum_{k=1}^{N_{fn}} \left(\int_{\Gamma_j} u^* \psi_k d\Gamma_j\right) \frac{\partial u_{kj}}{\partial n} = 0 \qquad (13)$$

The notation can be simplified by making use of matrix notation, so the last expression can be written in the following way:

$$\mathbf{H}[\mathbf{u}] - \mathbf{G}[\frac{\partial \mathbf{u}}{\partial \mathbf{n}}] = 0 \qquad (14)$$

where

$$H_{il} = \delta_{il}c_i + \int_{\Gamma_j} \left.\frac{\partial u_i^*}{\partial n_j}\right|_{\xi_j} \psi_k(\xi_j)d\Gamma_j, \qquad (15)$$

$$G_{il} = \int_{\Gamma_j} u_i^*(\xi_j)\psi_k(\xi_j)d\Gamma_j \qquad (16)$$

where $\mathbf{u} = u_l$ and $\partial\mathbf{u}/\partial\mathbf{n} = (\partial u/\partial n)_l$ are the potential and its normal derivative, respectively at l-th collocation node. Index $l = 1 \cdots N_{\text{fe}}$ (N_{fe} = total number of collocation nodes in Ω), denotes the total number of collocation nodes within the integration domain. In other words, l is used to label one of the adjacent freedom (collocation) nodes from a global point of view, and is given as a function of the element index (j), and the local collocation node of that element (k), i.e. $l = f(j, k)$, where f is the nodal connectivity function of the domain. The boundary element $d\Gamma_j$ can be expressed in terms of the domain local coordinates (ξ) through the Jacobian of the transformation $|J|$ in the following way:

$$d\Gamma_j = |J| d\xi_1 d\xi_2. \qquad (17)$$

Finally, provided that the right hand side term of equation (14) can be written as a given vector in function of the source term, or a characteristic matrix in function of the unknown potentials and normal fluxes at the collocation nodes of the boundary, the application of the prescribed boundary conditions and the assembly of the linear set of equations, that (14) produces, yields to a determined system of equations of dimensions $N_{fe} \times N_{fe}$ of the form

$$\mathbf{AX} = \mathbf{b} \qquad (18)$$

where the vector of unknowns ($\mathbf{X}$) contains the potentials and normal fluxes that were not prescribed as boundary conditions, the matrix A involves the coefficients of H and G, and the right hand side term involves the source term, and the boundary conditions.

3) Internal solution: Once the problem determined by matrix equation (18) is solved, it is possible to calculate the values of the fluxes ($\nabla u(\mathbf{x}_i)$) and potentials $u(\mathbf{x}_i)$ at any internal (observation) node $\mathbf{x}_i$ by means of the integral equation (8), and (9). Therefore, the potential at x_i becomes:

$$u_i = \sum_{j=1}^{N_{\text{fe}}} [\partial_n u_j] G_{ij} - \sum_{j=1}^{N_{\text{fe}}} u_j H_{ij} \qquad (19)$$

and the gradient of the potential can be computed as follows:

$$\left. \frac{\partial u}{\partial x_p} \right|_{x_i} = \sum_{j=1}^{N_{\text{fe}}} \int_{\Gamma_j} [\partial_n u_j] \frac{\partial u^*}{\partial x_p} d\Gamma_j -$$
$$\sum_{j=1}^{N_{\text{fe}}} \int_{\Gamma_j} u \frac{\partial}{\partial x_p} \left(\frac{\partial u^*}{\partial n} d\Gamma_j \right) d\Gamma_j. \qquad (20)$$

III. RESULTS AND DISCUSSION

Results obtained with the summarised formulation for ELF problems have been applied to the problem of a human body exposed to the electric field generated by overhead power lines.

A. Power Distribution Lines

This example considers a grounded human body located underneath a high voltage, three phase, three wire transmission line of $60\,Hz$.

The induced current in different conceptual models of the body is analysed. The main objectives of this study are first to compare the numerical findings between conceptual models that take into account different degrees of geometrical detail, and second to evaluate the influence of the relative position of the arms on the axial distribution of the current density along the head and torso.

The wires are located high enough so that to produce a uniform distribution of vertical electric field before getting close to the near field of the human body who stands in line with the wires. Analytical expressions of electric fields generated by transmission lines without the presence of any conducting body can be found in [16]. In particular, for power lines above $20\,m$ the vertical component E_z, which most affects the induced currents in the body, can be considered as nearly uniform in the region $0 < z < 10m$, $-5 < x(y) < 5$, when the wires are extended along $y(x)$ direction. In addition, a uniform electric field coming from the top onto a human being, will sense its influence not before $4\,m$ above the head, as seen in Figure 2(a) where the equi-potential lines in the air surrounding the body are nearly unaffected in the shaded area. The electric field along two vertical observation lines, one aligned with the standing man ($x = 0m$) and the other $5\,m$ away from him has been calculated with a two dimensional BEM code in order to approach to the 3D model. The solution is plotted in Fig. 2(b). By Keeping into account these assumptions, and trying to minimise as much as possible the size of the integration domain so to reduce the computational burden in the 3D model, it is reasonable to adopt a parallelepiped of approximately $5\,m$ height, $4\,m$ wide such as the unshaded region shown in Figure 2 (b) surrounding the human body. Hence, the 3D model considered in this work has the dimensions shown in Figure 1.

1) Human body modelling: Basically the human body is regarded as a saline fluid with conductivity $\sigma = 0.5\,S/m$. Five different conceptual models of the realistic human body, namely: CYL, HNA, HAO, HAU and HIO are considered in this work. Figure 3 summarises the main features of the conceptual models. CYL is a simplified model where the human body is represented by a cylinder of a diameter $0.364\,m$ and height $1.75\,m$. HNA is a more realistic model, which considers the arms attached to the body, as seen in Figure 3(c). HAO (Figure 3(a)) and HAU (Figure 3(b)) include the presence of arms. HAU considers arms extended making an angle of 60° with the horizontal plane. In the HAO model the arms are extended parallel to the horizontal plane. The
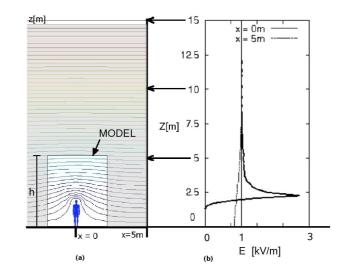

Fig. 2. Electric field in the air

conductivity is considered homogeneous in all the models, except HIO. HIO takes into account the presence of some relevant tissues like brain, eyes, heart, liver, kidneys, and intestine. All organs are treated as conductors embedded in a saline fluid with conductivity $0.5\,S/m$. The conductivities of those organs are relatively lower than its surrounding media. The values of conductivities used for different organs are shown in Table I. As a reference, in all the models the

Tissue Type	Conductivity (S/m)
Muscle	0.5
Heart	0.11
Brain	0.12
Eye	0.11
Liver	0.13
Kidney	0.16
Intestine	0.16

TABLE I

TISSUE CONDUCTIVITIES USED AT ELF EXPOSURE.

origin of the coordinates system is represented by the point "O" of Figure 3(a) .

Average values of physical and geometrical properties have been obtained from available databases and references: [13],[7], [6], [17] and [14].

The preprocessing and the geometrical introduction represented a major problem which has been sorted out by adapting a customizable geometry modeller, pre-processor and mesh generator [18]. The meshes generated have a number of elements ranging between 4,000 to 20,000. For example, in the HNA model the mesh has nearly 4,000 elements.Whereas, the number of elements in the HIO model is nearly 18,000. In the HAO and HAU models the number of elements is also in the order of 18,000.

2) Analysis of the refinement of geometry. Comparison between the models CYL and HNA : Figure 4 shows the results of the induced axial current density (j_z) calculated along the longitudinal axis z of the human body for both models CYL and HNA. The calculation line passes through the centre of the body in the region between $z = 1.75$ to $z = 0.85$. Below $z = 0.85$ the calculation line passes through the center of one leg. In the HNA model four well identified peaks appear at the levels of the neck, waist, knee, and ankle. Hence, an oversimplified representation of the human body such as the cylindrical or ellipsoidal models are unable to capture the effect of high current densities in regions of reduced cross section. Peak values are summarised in Table II. Results
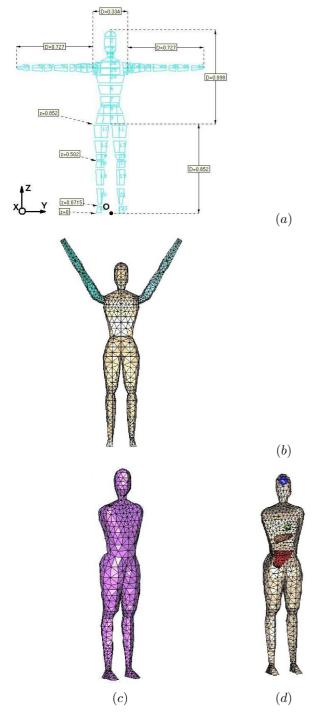
Fig. 3. Meshes and Dimensions for the Human Body Models. General Features of the Conceptual Models for human body (a) HNA, (b) HAO, (c) HAU, (d) HIO

Height	$\mathbf{j_{z\,HNA}}[mA/m^2]$	$\mathbf{j_{z\,CYL}}[mA/m^2]$
Neck	9.8	0.87
Knee	8.6	1.59
Ankle	32	1.98

TABLE II

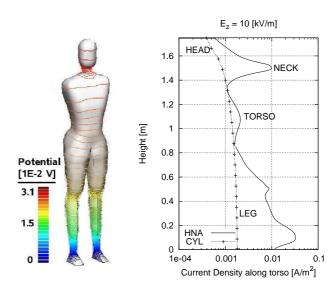PEAK VALUES OF AXIAL CURRENT DENSITY FOR HNA AND CYL MODELS

Fig. 4. Axial component of the current density vector along the the human body for the models CYL and HNA

obtained are comparable with the ones obtained by different methods and presented in earlier publications such as [6] , [7] and [9].

3) Analisis of the inclusion of arms: Global results can be seen in Figure 5(a), where equipotential lines are shown in the near field zone of the grounded human model with the arms raised (HAU), exposed to a planar field.

A 3D view of the complete model (HAU) showing the density plot of the scalar potential φ can be seen in Figure 5(b). Figure 6 compares the axial current distribution (j_z) along a vertical line in z direction that passes through the centre of the head and torso. The comparison is done between the models: HAU, HAO and HNA, corresponding to the human body with the arms up, horizontally extended and no arms at all, respectively. Table III shows the corresponding peak values of current density for the different models, which are typically found in the neck. It can be observed that when both arms are extended

Model	Peak $\mathbf{j_z}[mA/m^2]$
HAU	11.8
HAO	11.8
HNA	4

TABLE III

PEAK VALUES OF AXIAL CURRENT DENSITY IN THE TORSO FOR THE

THREE DIFFERENT MODELS

upwards, the peak can decrease to approximately 35% of the value with the arms either extended horizontally or attached to the body, thus causing the expected screening effect. In the region between $z = 0.85$ and $z = 1.4m$ (torso), the smallest values of $j_z \sim 2mA/m^2$ to $3mA/m^2$ can be found when the arms are attached to the body. Finally, from all point of view, the maximum values of induced current are found when both arms are perpendicularly oriented to the incident vertical field.

4) Analysis of the inclusion of organs: Figure 7 shows a comparison between the induced currents in models HIO and HNA. This comparison has been done in order to estimate the influence of the internal organs showed in Table I on the induced axial current along the torso. The conductivity of the internal organs are relatively lower than the conductivity of the medium in which are embedded, thus yielding some local depressions of current density observed between $0.8m$ and $1.3m$. The observation line, which extends from $(x, y, z) = 0, 0, 0.82$ to $(x, y, z) = 0, 0, 1.75$, interferes with the intestine between $z = 0.93m$ and $z = 1.07m$ (points A and B, respectively), hence the first depression observed in the figure. Then,
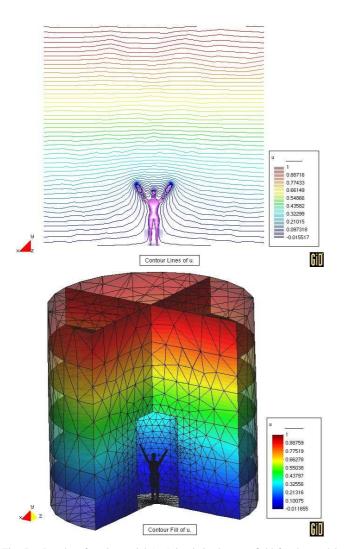
Fig. 5. Results of equipotential (top) in air in the near field for the model HAU (bottom)
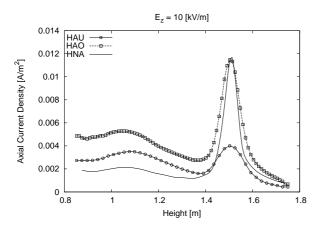

Fig. 6. Axial current density along the torso and head in function of the height for the HAU, HAO and HNA models.

the current rapidly increases in the subsequent region of higher conductivity until it reaches the liver at point C which causes another depression between $1.15m$ and $1.2m$. Although the heart does not interfere with the observation line, its presence can be sensed near $z = 1.28m$ (point C) where it is at its minimum distance of nearly $2cm$. Therefore, due to its lower conductivity, the heart will cause a local maximum in the adjacent region considered as a saline solution (point D). Furthermore, in this model the value of axial current density computed at the centre of the heart is given by:

$$j_z^{(\text{heart})} = \alpha E_z, \qquad (21)$$

where $\alpha = (4.4 \pm 0.1) \times 10^{-8} A\ V^{-1} m^{-1}$, and E_z is the vertical electric field at ground level measured without the human body (i.e. $0.4mA/m^2$ underneath a $10kV/m$ power line). The peak at point E is correlated to the reduction of the cross section in the neck and its value is insensible to variations on the location and conductivities of the internal organs. Then, the current density decreases as the exposed cross section increases from the neck to the centre of the head. Finaly, the last depression is found between points E and G due to the lower conductivity of the brain.

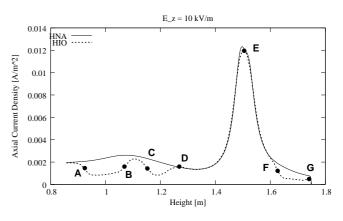As observed in Figure 7, the HNA model gives an envelope of the HIO.

Fig. 7. Axial current density along the torso and head in function of the height for the HAU, HAO and HNA models.

IV. CONCLUSION

The paper deals with the realistic 3D model of the human body exposed to ELF electric fields, based on the Boundary Element analysis. The formulation of the electromagnetic problem has been based on the assumptions of high intensity electric fields at ELF. Solving the Maxwell's equations under these assumptions, the electromagnetic problem has been reduced to a set of piecewise homogeneous Laplace's equations for the scalar potential. After solving them the electric field induced in the body and the current distribution inside the body can readily be derived. In this way, a 3D flexible BEM method has been applied to analyze human exposure to ELF electric fields featuring the non homogeneous representation of the human body. The formulation provides more accurate results than standard methods since it is based on the fundamental solution of the leading operator for the governing equation. The results obtained show that a simplified cylindrical model of the human body is useful for determining orders of average values of current densities in the torso, but it is not able to predict the maximum characteristic peak values that appear typically in neck, knees and ankles. In addition, those values are insensible to variations of physical and geometrical properties of the internal organs. It is important to stress that the external field solution is insensitive to the internal structure of the human body. In addition, the vertical profile of current density is strongly dependent on the external shape and narrowing of the human body and relatively insensitive to the shape and location of major internal organs.

References

[1] I. N. R. C. of the International Radiation Protection Association. Guidelines for limiting exposure to time-varying electric, magnetic, and electromagnetic fields (up to 300 ghz). *Health Physics.* 74(4):494–522, 1998.

[2] N. Burais, P. Baraton, and J. Gaspard. Numerical modelisation of induced currents in human by electromagnetic apparatus in medium frequency range. pp. 457–469, 1998.

[3] D. Poljak and V. Roje. Currents induced in human body exposed to the power line electromagnetic field. *Proc. 20th Annual Conference of the IEEE Engineering in Medicine and Biology Soc.*, pp. 3281–3284, 1998.

[4] A. Bossavit. Mathematical modelling of the problem of micro-currents generated in living bodies by power lines. *Int. J. Applied Electromagnetics in Materials* 4(4):291–99, 1994.

[5] P. Baraton and B. Hutzler. Calculation of current densities induced in the human body by a 50 hz magnetic field. *EBEA 3rd Int. Cong.*, p. 8, 1996.

[6] O. Gandhi and J. Chen. Numerical dosimetry at power line frequencies using anatomically based models. *Bioelectromagnetics Suppl.* 1:43–60, 1992.

[7] A. Chiba, K.Isaka, Y.Yokoi, M.Nagata, M. Kitagav, and T. Matsuo. Application of finite element method to analysis of induced current densities inside human model exposed to 60hz electric field. *IEEE Trans. Power Apparatus and Systems* 103(7):1895–1901, 1984.

[8] C. Brebbia, J. C. Telles, and L. C. Wrobel. *Boundary Elements Techniques*. Springer-Verlag, Berlin, Heidelberg New York and Tokio, 1984.

[9] D. Poljak, A. Peratta, and C. A. Brebbia. A 3D BEM modelling of human exposure to ELF electric fields. *Boundary Elements XXVII, Incorporating Electrical Engineering and Electromagnetics*, pp. 441–451, 2005.

[10] M. C. Gonzalez, A. Peratta, and D. Poljak. Boundary Element Modelling of the Realistic Human Body Exposed to Extremely Low Frequency (ELF) Electric Fields: Computational and Geometrical Aspects. *IEEE, Transactions on Electromagnetic Compatibility* 49(1), February 2007.

[11] J. Jackson. *Classical Electrodynamics*. J.Willey & Sons, New York, 1975.

[12] N.Siauve, R. Scoretti, N. Burais, L.Nicolas, and A. Nicolas. Electromagnetic fields and human body: a new challenge for the electromagnetic field computation. *Compel: The International Journal for Computation and Mathematics in Electrical and Electronic Engineering* 22(3):457–469, 2003.

[13] O. Gandhi. Some numerical methods for dosimetry: Extremely low frequencies to microwave frequencies. *Radio Sci.* 30(1):161–177, 1995.

[14] R.W.P.King. A review of analytically determined electric fields and currents induced in the human body when exposed to 50-60 hz electromagnetics fields. *IEEE Trans.on Antennas and Propagation* 52(5):1186–1192, 1998.

[15] C. Brebbia and J. Dominguez. *Boundary Elements, An Introductory Course. Second Edition*. Computational Mechanics Publications, McGraw-Hill, New York Colorado San Francisco Springs Mexico Montreal Oklahoma City San Juan Toronto, 1992.

[16] R.W.P.King. Currents and electric fields induced in the human body when the arms are raised. *J. Appl. Phys.* 81(11):7116–7128, 1997.

[17] R. King and S. Sandler. Electric fields and currents induced in organs of the human body when exposed to ELF and VLF electromagnetic fields. *Radio Sci* 31:1153–1167, 1996.

[18] CIMNE, International Center for Numerical Methods in Engineering. GID resources. Website. http://gid.cimne.upc.es.

María Cristina Gonzalez received her MSc in Physics in 1996 from University of Buenos Aires (Faculty of Exact and Natural Sciences), Argentina. Her background is in Numerical Modelling applied to Electromagnetic problems. She developed her graduate thesis at the Plasma Physics Institute, (INFIP), University of Buenos Aires-CONICET, Argentina, in numerical modelling applied to Nuclear Fusion in Z-pinch experiments. She is currently a Ph.D researcher at the Wessex Institute of Technology. Her thesis is oriented to numerical modelling applied to human exposure to electromagnetic fields.

Andrés Peratta received his MSc in Physics in 2001 from University of Buenos Aires, Argentina, and his PhD in 2004 from University of Wales, UK. During 2005 he has been a Postdoctoral Fellow and Assistant Professor at the Wessex Institute of Technology (WIT), Southampton UK and became member of the Editorial Board of Journal of Communications, Software and Systems (JCOMSS) sponsored by IEEE and SoftCom Society. In 2006 he became Head of the ICE Division at Wessex Institute of Technology and ISAC member of the WIT International Conferences on Environmental Electromagnetic Compatibility, Simulation of Electrochemical Processes, and Computational Ballistics. His research interests are Numerical Modelling, Boundary and Finite Element methods, Electromagnetism, Computational Fluid Dynamics and Continuum Mechanics.

Dragan Poljak received his BSc in 1990, his MSc in 1994 and PhD in 1996 from the University of Split, Croatia. He is the Full Professor at the Department of Electronics at the University of Split, and he is also Adjunct Professor at Wessex Institute of Technology, UK. His research interests include frequency and time domain computational methods in electromagnetics, particularly in the numerical modeling of wire antenna structures, and recently numerical modeling applied to environmental aspects of electromagnetic fields. To date Professor Poljak has published more than 180 journal and conference papers in the area of computational electromagnetics, four authored books and one edited book, by WIT Press, Southampton-Boston. Professor Poljak is a member of IEEE, a member of the Editorial Board of the journal Engineering Analysis with Boundary Elements, and co-chairman of the WIT International Conference on Computational Methods in Electrical Engineering and Electromagnetics, and International Conference on Environmental Electromagnetics. He is also editor of the WIT Press Series Advances in Electrical Engineering and Electromagnetics. Recently, professor Poljak was awarded by the National Prize for Science.